Bubble cavity for ethylene encapsulation based on starch-fatty acid salt complex

Zhanpeng Liu [a,c], Yi Jiang [a], Bin Zhang [a,b], Xiong Fu [a,b], Qiang Huang [a,b*], Paul Van der Meeren [c]

[a] SCUT-Zhuhai Institute of Modern Industrial Innovation, School of Food Science and Engineering, South China University of Technology, Guangzhou 510640, China

[b] Overseas Expertise Introduction Center for Discipline Innovation of Food Nutrition and Human Health (111 Center), Guangzhou 510640, China

[c] Particle and Interfacial Technology Group (PaInT), Department of Green Chemistry and Technology, Faculty of Bioscience Engineering, Gent University, Coupure Links 653, Gent 9000, Belgium

---

[*] Corresponding author.

E-mail: qiangh@scut.edu.cn (Q. Huang).

Abstract: This study investigated the effects of bubble or bubble gel characteristics on gas loading properties. The bubble carriers prepared by starch-fatty acid salt (SFAC) complex presented a better loading ability for ethylene with content in the range of 0.43-0.95 mL/g, in which bubble system prepared by 4% SFAC dispersion showed a better gas loading performance (0.95 mL/g). The gas content significantly decreased to 0.22–0.66 mL/g after bubble gel formation. However, all bubble gel had a slower gas release rate than that of corresponding bubble. In bubble gel system, bubble cavity immobilized with a gel network to reduce bubble breakage and coalescence, which was beneficial for retarding gas escaping. Besides, water layer surrounded by bubble cavity, as a physical barrier, could further slow gas-escaping speed. As an effective carrier, the bubble and bubble gel carriers based on starch are potential material for ethylene gas encapsulation used in fruit ripening applications.

Keywords: starch, ethylene, gas encapsulation, bubble, bubble gel, release

1. Introduction

The uncontrollable risks of ethylene gas, usually directly used in ripening process (Huang et al., 2020) led researchers to utilize cyclodextrins (CDs) (Binh et al., 2015), metal-organic frameworks (MOFs) (Zhang et al., 2016), and V-type starch (VS) (Liu et al., 2022a; Liu et al., 2022b; Shi et al., 2017a) as solid carriers to encapsulate ethylene gas. The CD molecule showed about 2.9% (w/w) of ethylene loading capacity at 0.2–1.5 MPa with the help of hydrophobic interactions (Ho et al., 2011). However, the fixed cavity size of CD limited its loading ability. The large internal surface areas and tunable cavities of the MOF based α-CD significantly improved the capacity, and encapsulation ability of the ethylene gas was to 47.4–52.9% (w/w) (Li et al., 2020). Meanwhile, the flexible hydrophobic hollow structure of the VS contributes to the ethylene gas encapsulation (Shi et al., 2017b). The VS cavity size is classified to V_6, V_7, and V_8-type, depending on the number of glucose units (Shi et al., 2019a). The loading performance of VS is significantly correlated with the percentage of V-type single helix. Our previous study reported that ethylene concentration increased from 8.0–31.8% (w/w) to 18.1–49.6% (w/w) because of an increase in the V-type single helix ratio (Shi et al., 2019b). However, these existing materials have many practical disadvantages, such as poor stability (VS), low adsorption capacity (CD), and high cost (MOF). Hence, it is important to develop novel ethylene carrier that is in line with the needs of practical applications.

Bubbles are a natural form of gas surrounded by liquid or solid substances to form spherical cavity bubbles. According to their diameter, bubbles are divided into nanobubbles, sub-microbubbles, and microbubbles (Temesgen et al., 2017). The nanobubbles have been widely used in water treatment (Temesgen et al., 2017), medical imaging, drug delivery (Lindner et al., 2001; Shen et al., 2018), surface cleaning, and mineral flotation (Wu et al., 2008; Zhu et al., 2016) for the past 20 years due to their excellent stabilizing and functional properties. In the process of water treatment, ozone-loaded nano- or microbubbles provide more active free radicals and oxidants to purify wastewater efficiently (Agarwal et al., 2011; Jay et al., 2017; Hu and Xia, 2018). In the field of medical imaging, microbubbles penetrate into blood vessels, and the health of blood vessel tissues is assessed by ultrasound feedback under the action of some target-binding receptors found on the bubble surface (Lindner et al., 2001). In the pharmaceutical industry, bubbles with high stability, good biocompatibility, and uniform particle size were used to deliver oxygen (O_2) (McEwan et al., 2015), nitric oxide (NO) (Jeong et al., 2018), and xenon (Xe) (Peng et al., 2013). In the medical field, the nano- or microbubble carrier (Friedman et al., 2008) requires high production technology and cost. However, in the fruit ripening process, the bubble carrier has no such demands. Furthermore, the ethylene gas encapsulation into bubbles or bubble gel has not been reported.

In this study, the ability of bubbles to carry ethylene was investigated based on the starch-fatty acid salt complex (SFAC). In addition, the bubbles were immobilized into bubble gel matrix for enhancing bubble cavities stability. It was hypothesized that ethylene gas could be encapsulated in bubble or bubble gel carrier in a storage environment. Therefore, the characteristics of bubble and bubble gel, including bubble diameter, microstructure of bubble gel, gas loading capacity, and storage stability, were investigated. Bubble or bubble gel carrier could efficiently promote fruit and vegetable ripening development.

2. Materials and methods

2.1. Materials

SFAC was prepared using normal maize starch (5 %, w/w) and sodium laurate (10 % of the weight of starch) in laboratory (Jiang et al., 2023). D-(+)-gluconic acid δ-lactone was purchased from Shanghai Aladdin Co., Ltd. (China). The Gaonengda Chemical Industry Co., Ltd. (Zhaoqing, China) provided the ethylene gas (99.9% purity). All other chemicals used were of analytical grade.

2.2. Ethylene in a water bubble system preparation

The bubble system prepared according to the previous research (Liu et al., 2019) with slight modifications. Briefly, appropriate weight of SFAC was dispersed in 100 mL water to obtain 2%, 3%, 4%, 6% dispersion followed by addition of Tween 80 (1%, w/w) as emulsifier. The ethylene gas was injected continuously into the dispersion bottom to gain an ethylene environment. Meanwhile the system was high-speed shear treatment at 20,000 rpm for 2 min to prepare bubble system. The resulting bubbles were immediately analyzed and detected.

2.3 Preparation of bubble gel

SFAC dispersion formed a gel network after contacting with H^+ (Jiang et al., 2023). To hold ethylene gas and enhance stability of bubble cavities, the bubble gel matrix was prepared by addition of the d-(+)-gluconic acid δ-lactone to release H^+, generat an acid environment, and form a bubble gel. Thus, fresh bubbles (100 mL) were mixed with 0.1 g d-(+)-gluconic acid δ-lactone followed by stirring and solidification for 10 min to form bubble gel carrier.

2.4 Characteristics

2.4.1 Microscopic observation

An inverted microscope (DMi8, Leica, Germany) was used to observe the microscopic images of bubbles at ambient temperature under bright mode. A certain volume of bubble dispersion (about 30 μL) was dropped in microscope slide glass and images of samples were observed at 10×40 magnification.

2.4.2 Size distribution of bubbles

The bubble diameters and size distribution determined using ImageJ software (v1.51, National Institute of Health, USA). The diameters were calculated through pixel analysis according to the scale bars. At least 100 bubbles were selected to evaluate the diameters and size distribution data.

2.4.3 The viscosity analysis for dispersion and bubble system

The SFAC dispersion and bubble system were tested by a Discovery HR-1 rheometer (TA Instrument Ltd., USA) at 25 °C. The shear rate of viscosity tests for samples were set from 0.1 to 100 s^{-1}. The functions of shear stress and shear rate was described by the Power-Law and Herschel-Bulkley (HB) models (Fan et al., 2022).

Power Law model: $y = k(x)^n$ Eq (1)

HB model: $y= a + k(x)^n$ Eq (2)

where y represent the shear stress (Pa) of the dispersion and bubble, x is the shear rate (s^{-1}), k is the consistency (Pa·s), and n is the flow behavior index.

2.4.4 Viscoelastic detection

A Discovery HR-1 rheometer (TA Instrument Ltd., USA) was used to detect viscoelastic characteristics of bubble gel. In this section, the non-bubble gels were formed by corresponding SFAC dispersion as control groups. On strain sweep and frequency sweep modes, the storage modulus (G′) and loss modulus (G″) of samples were detected. The frequency sweep was set to 0.1–100 Hz at a specific 1% strain. The strain sweep operation was set to the 1%–100% strain at a frequency of 1 Hz. All the operations for samples and detection were set at 25 °C.

2.4.5 Morphology observation

The morphology of samples observation used to a scanning electron microscope equipment (Phenom Pro, Thermo Fisher Scientific Inc., Waltham, USA). The dry bubble gel and non-bubble gel were fixed on microscope stage with conductive double-sided tape. In order to increase conductivity of samples, gold layer (10 nm) was sprayed on the surface.

2.5 Gas loading ability and stability

According to our previous report, the ethylene content of samples was detected (Shi et al., 2017a). In brief, 0.5 g bubble or bubble gel were placed into an sample vial, subsequently adding 1 mL of water. The cap was sealed immediately. To thoroughly release ethylene gas, all sample vials were shaken for 5 min. The headspace gas chromatography (HS-GC) was used to determin ethylene content, which equipped with an Agilent 7890A GC system (Agilent, CA, USA). At the same time, the sample injection was used a DANI HS 86.50 automatic headspace sampler (DANI Instruments S.p.A., Cologno Monzese, Italy).

2.6. Statistic analysis

All experiments operation were at least three times. The SPSS 20.0 statistical analysis program (IBM Corp., USA) was used to obtain the analysis of variance (ANOVA) of the data. The difference among samples was judged by the Duncan's post hoc test. When *p* values were < 0.05, differences between data were considered statistically significant.

3. Results and discussion

3.1. The microstructure and size distribution of bubble

The observed micrograph images of fresh bubbles are shown in Fig. 1. The bubble diameter of individual bubbles of different SFAC concentrations decreased gradually from 47.8 μm to 26.2 μm with the increase in SFAC concentration from 2% to 4%, while the bubble size of 6% SFAC concentration increased significantly. A previous study reported that the SFAC could act as emulsifier to form oil in water emulsion (Huang et al., 2021), which indicated its emulsifying properties. Thus, with an increase in the concentration (2–4%) of SFAC, the bubble diameter decreased. While the larger bubble size formed in the 6% SFAC system might be due to the higher viscosity that hindered energy dispersion (Schmidt et al., 2015).

Fig. 1 shows the size distributions of fresh bubble. The diameter of 2% SFAC bubbles ranged from 15–120 μm (Fig. 1a), while the size of 3% and 4% SFAC decreased to 5–90 μm and 5–65 μm after stabilization, indicating that 2–4% SFAC concentration relatively showed uniform particle size. However, a wide range of size distribution was obtained in the 6% SFAC bubble system, leading to a bigger average bubble diameter (43.3 μm), consistent with microscope images (Fig. 1). After 60 h of storage, all bubbles disappeared (data not shown), which was ascribed to the burst and coalescing among bubbles. A previous study reported that the stability of gaseous bubbles depends on the bubble size (Zahiri et al., 2021), in which nanobubbles usually maintain stability. For example, bubbles with a 150–200 nm diameter can be stably stored in a solution system for 2 weeks (Azevedo et al., 2016). That means that the microbubble was hard to stabilize because of its tendency to float up. In this study, the size of a fresh bubble was in the range of 26.2–47.8 μm, which was much larger than nanobubbles. Moreover, the wide range of diameter distribution could have an effect on bubble stability. The large bubble had an imbalanced force, leading to intensified movement and coalescence, which also accelerated bubble breakage. In addition, many factors could also affect the stability of bubbles (Zahiri et al., 2021), especially system viscosities. Thus, in this research, the viscosities of SFAC dispersion and the corresponding bubble were detected to further investigate the bubble stability.

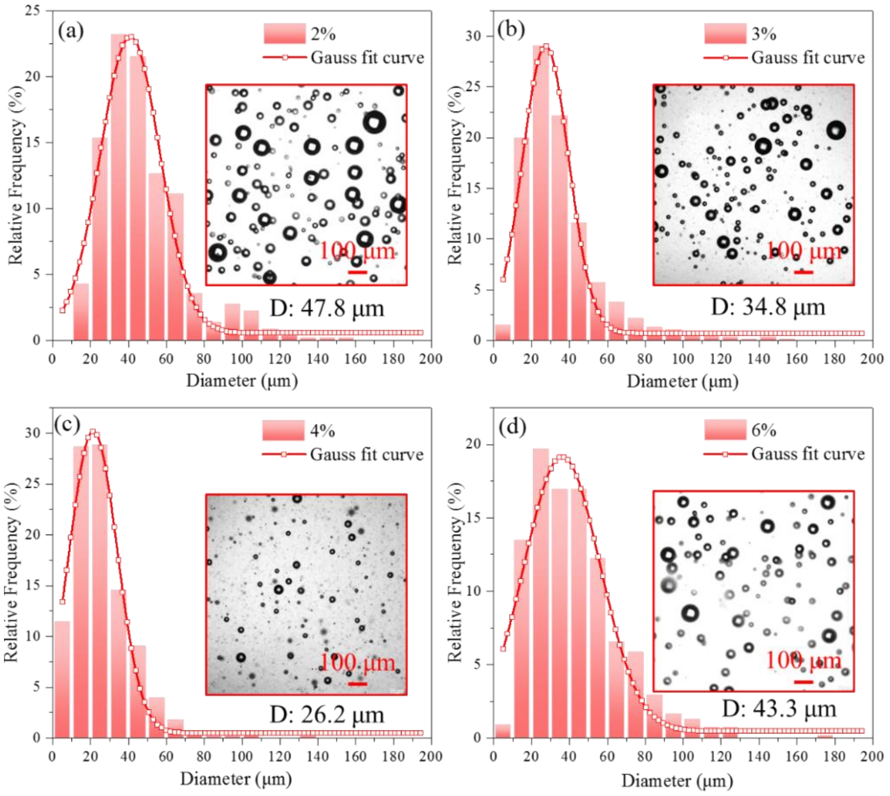

Fig. 1 The size distribution and micrographs of fresh bubble system prepared by 2% (a), 3% (b), 4% (c), and 6% (d) starch dispersion.

3.2 The shear stress and viscosity of dispersions and bubbles

The changes in the viscosity and shear stress of the SFAC dispersions and corresponding bubbles are shown in Fig. 2. The viscosity of both dispersion and bubble samples increased with an increase in SFAC concentrations, consistent with a previous study (Islam and Azemi, 1997). The higher SFAC concentration showed a higher molecule density and lower water penetration with restricted mobility and fluidity. According to previous studies (Liu et al., 2020), the influence of viscosity on emulsification could be divided into two parts, similar to the bubble system (ethylene gas in water emulsion). On the one hand, a higher viscosity of dispersion could retard the emulsifier's movement to the interface, decreasing the emulsifying activity. As shown in Fig. 2a, the 6% SFAC had the highest viscosity, which limited Tween 80 movement to surface during bubble formation under the same conditions, resulting in the formation of a larger diameter bubble. On the other hand, the bubble movement might be restricted because of a higher viscosity, which is useful for maintaining bubble stability, similar to the oil-in-water emulsion reported by a previous study (Schmidt et al., 2015). In addition, it could be clearly seen from Fig. 2a that the viscosity of the bubble system was higher than that of the counterpart dispersion, which might be due to the decreasing intermolecular distance between SFAC molecules, enhancing the entanglement network, and consequently having higher viscosities in the bubble system.

The viscosities of SFAC dispersion and corresponding bubble decreased with the increasing shear rate (Fig. 2a), exhibiting shear thinning characteristics. A previous study explained this phenomenon (Islam and Azemi, 1997), in which the rate of disruption of the existing entanglements among starch molecules was higher than the rate of re-entanglement, resulting in decreasing viscosities. Compared to dispersion, the viscosities of the bubble system had a faster decreasing speed, which could be attributed to the breakage of the bubble cavity during viscosity detection. These results indicated that stronger pseudoplastic behavior was obtained in all dispersion and bubble systems. These results were agreement with previous researches (Muhammad et al., 2014; Chan et al., 2017; Dodero et al., 2020), in which Newtonian behavior was obtained at a lower pectin concentration and pseudoplastic behavior was observed at higher polysaccharide concentrations. This is a common phenomenon for polysaccharides.

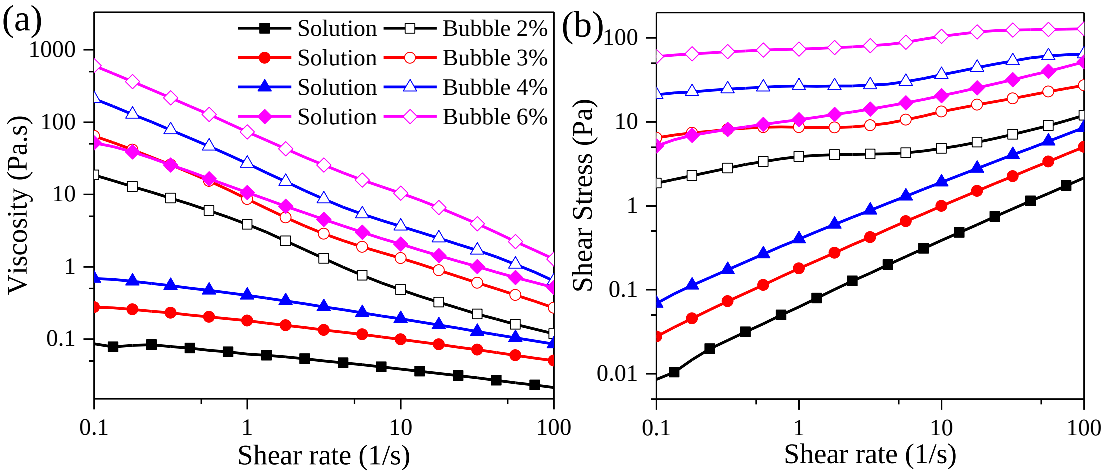

Fig. 2 The changes in the viscosity (a) and shear stress (b) of dispersion and bubble system with the shear rate

The shear stress of dispersions and bubbles increased slowly with the increase in shear rate (Fig. 2b), consistent with previous research (Nascimento et al., 2016). Besides, the bubble had a higher shear stress compared to its counterpart dispersion. In order to further analyze rheological behavior, the data between shear stress and shear rate was fitted by the Power Law and HB models, and Table 1 shows the functional parameters. The parameters *k* and *n* represented the apparent viscosity and flow behavior index (Fan et al., 2022; Yanes et al., 2002), respectively. From Table 1, with an increase in the SFAC content, the apparent viscosity (*k* value) of dispersion and bubble systems increased and the flow behavior index (*n* value) decreased. The same results obtained by two different fitting equations indicated that interactions among SFAC molecules were enhanced with an increase in concentration. Compared to dispersion, the corresponding bubble had a higher *k* value and a lower *n* value, suggesting that molecules in the bubble system had a restricted movement space. These results could be attributed to the fact that SFAC molecule interaction was enhanced after bubble cavity formation, leading to an increase in the *k* value and a decrease in the *n* value of SFAC molecules. In addition, the *n* values of all dispersion and corresponding bubble samples are less than 1, which indicates that all samples belong to pseudoplasticity fluids (Fan et al., 2022), consistent with the results of Fig. 2.

Table 1 Rheological parameters of dispersion and bubble systems fitted by the Power Law and HB models in steady flow behavior.

Smaples ID		Power law model			HB model			
		K (Pa. S)	n	R^2	a (Pa)	K (Pa. S)	n	R^2
Dispersion system	2%	0.069	0.747	0.999	0.005	0.071	0.741	0.999
	3%	0.194	0.707	0.999	0.014	0.201	0.700	0.999
	4%	0.421	0.653	0.999	0.027	0.436	0.646	0.999
	6%	9.510	0.358	0.991	0.258	9.234	0.363	0.991
Bubble system	2%	3.167	0.256	0.952	1.196	1.797	0.367	0.962
	3%	8.764	0.226	0.941	4.679	3.402	0.412	0.973
	4%	26.788	0.184	0.933	12.648	12.483	0.321	0.952
	6%	74.972	0.131	0.939	50.036	126.698	0.081	0.942

3.3. Analysis of rheological characteristics of gel

Above results indicated that microbubbles based on SFAC were hard to hold stability. Thus, bubble gel was prepared to immobilize the bubble cavity, which could reduce bubble mobility and breakage. Meanwhile, to confirm the effect of bubbles cavities on the gel rheological characteristics, the non-bubble gels prepared by the corresponding SFAC dispersion were used as reference samples. The bubble gel formation mechanism was reported by previous research (Jiang et al., 2023). Briefly, the negative charge of SFAC molecules repel each other to form sol state in water system. The negative charge of SFAC neutralized with d-(+)-gluconic acid δ-lactone, gradually released the H^+, and transferred the sol dispersion into gel state.

Fig. 3 shows the strain sweep curves and oscillatory frequency sweep curves. Compared to the loss modulus (G″) value (Fig. 3a and b), the non-bubble gel and bubble gel prepared by 2% SFAC had a higher storage modulus (G′) value, and also the G′ value of samples at 1% oscillation strain was lower than 130 Pa, which was significantly lower than that G′ value of 1% gellan gum (500 Pa) (Fan et al., 2022), indicating weak gel formation in the 2% SFAC dispersion and bubble systems (Ferreira et al., 2022; Chen et al., 2023). In addition, according to previous study (Chen et al., 2021), the G′ represented hardness and G″ values represented the energy consumption to resist flow in the gel system. As shown in Fig. 3a and b, the G′ and G″ values of all samples increased with SFAC content increasing, indicating that non-bubble gel and bubble gel had a higher hardness and energy consumption at higher SFAC concentrations. This phenomenon could be ascribed to different densities of junction zones or chain-chain interactions among SFAC molecules at different SFAC contents (Koev et al., 2020; Dudu et al., 2021). The higher SFAC concentration formed more junction zones after electrostatic repulsion elimination, leading to higher G′ and G″ values.

The strain sweep curve could gain the critical linear viscoelastic region (LVR), which could analyze the limit G′ value (Nair and Roy Choudhury, 2020). The nonlinear deformation in the curve appeared after exceeding the LVR point, indicating samples yielding. Interestingly, yield stress of both gel and bubble gel systems obtained by 2% SFAC were the highest (Fig. 3a and b). This might ascribe to the starch chain structure in the gel network linked by junction zones in 2% SFAC had more movement space, which could reduce the destruction of the gel network below a certain strain during detection. While the yield stress of a 3–6% gel or bubble gel system having no significant difference, which might be attributed to the starch chain in the system having a similar movement space.

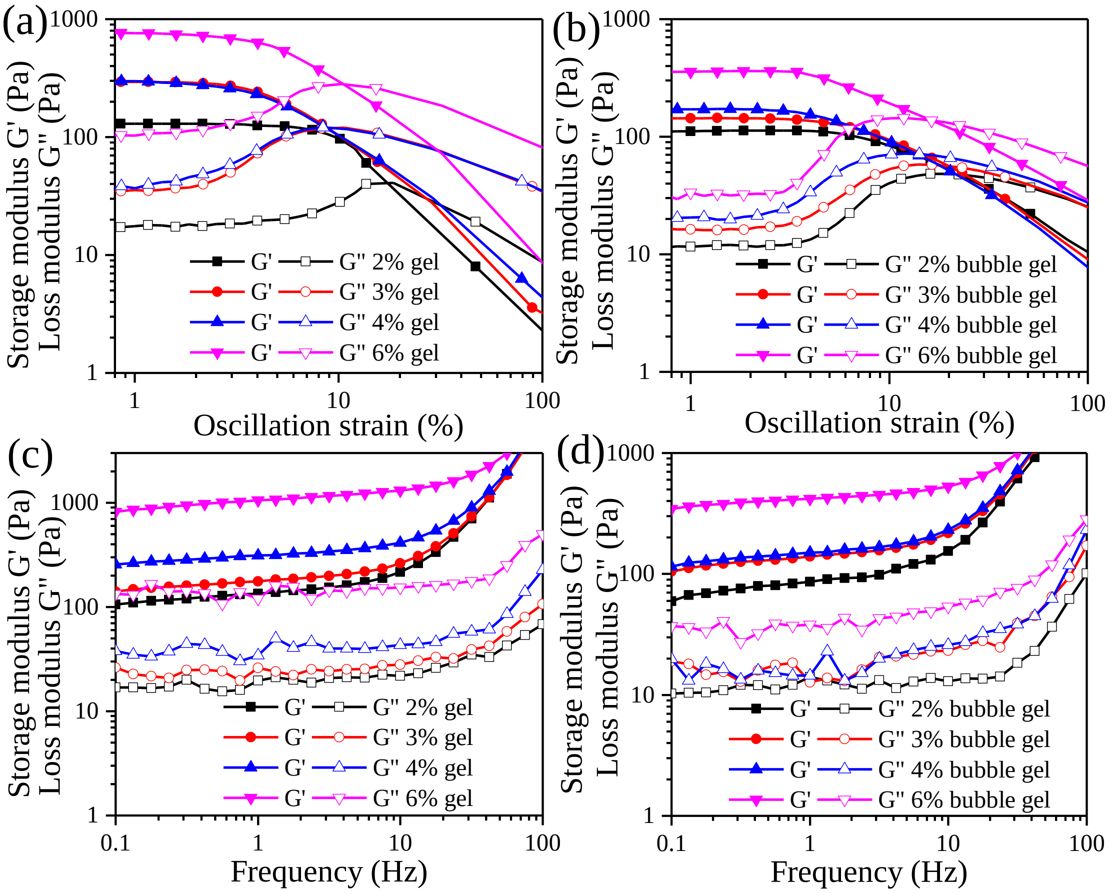

Fig. 3 The strain sweep curves of gel (a) and bubble gel (b) system and the oscillatory frequency sweep curves of gel (c) and bubble gel (d) system.

Fig. 3c and d shows the oscillatory frequency sweep curves of non-bubble and bubble gel, in which could obtain the modulus and the tanδ (G″/G′) values. The frequency sweep curves of all samples showed higher G′ values than G″ and the tanδ values of all gels were less than 1. These results indicated that all gel samples maintained an ideal elastic state in detecting frequency ranges (Arogundade et al., 2021; Fan et al., 2022). Similarly, in the strain sweep curves, the G″ and G′ values still showed a gradual increase in the SFAC concentration and frequency sweep mode (Fig. 3c and d), further indicating the improvement of junction zones with an increase in SFAC concentration.

3.4. The morphology of bubble gels

To obtain information on gel and bubble gel structures, the surface of all samples was examined after the lyophilization. The gel and bubble gel structures prepared by 2% SFAC hardly maintained the blocky structure after lyophilization, thus it could not be observed in this section.

The SEM images of non-bubble gel and bubble gel prepared at different SFAC concentrations (3–6%) are shown in Fig. 4. The non-bubble gel matrices (Fig. 4a, c, and e) formed after SFAC molecules were contacted with H^+. It can be seen from micrographs that all non-bubble gels presented a porous structure, which was due to solvent evaporation during lyophilization, accordance with a previous study (Montes et al., 2022). Besides, the porous size gradually decreased with an increase in the SFAC from 3–6%, which might be ascribed to an increase in the SFAC density, leading to the formation of more junction zones. However, the bubble gel showed different morphology with different sheet structures (Fig. 4b, d, and f). This phenomenon could be attributed to the presence of bubble cavities, which could affect the accumulation of SFAC during gel formation. Compared to bubble gel formed by 3% SFAC, bubble cavity structure was obviously observed in 4% and 6% bubble gel matrices, which directly proved the bubble presence in bubble gel. In addition, according to this microstructure discrepancy, the non-bubble gel structure-maintained integrity is linked with junction zones, which might lead to a higher G′ and G″ value, further proving the rheological results (Fig. 3).

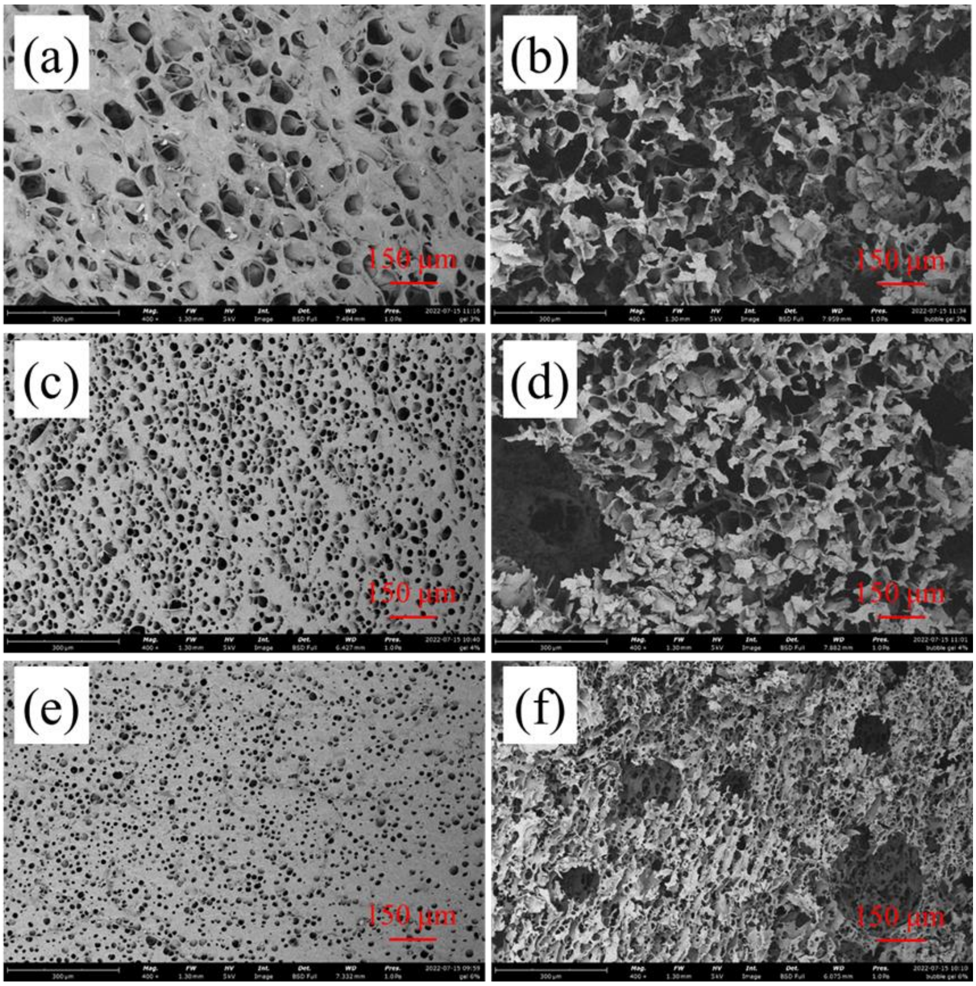

Fig. 4 SEM images of gel system prepared with 3% (a), 4% (c), and 6% (e) starch dispersion, and bubble gel system prepared with 3% (b), 4% (d), and 6% (f) starch bubble system.

3.5 Gas encapsulation capacity and release for carriers

Fig. 5 showed the ethylene gas content in fresh bubble, bubble gel system, and gas release at atmospheric temperature. As shown in Fig. 5a, the fresh bubble obtained with 3%

SFAC had the highest ethylene content (0.95 mL/g), the following order is 2% SFAC (0.86 mL/g), 4% SFAC (0.81 mL/g), and 6% SFAC (0.43 mL/g). After gel formation, gas encapsulation content significantly decreased compared to the counterpart bubble system. The bubble gel prepared with 3% and 4% SFAC loaded 0.66 mL/g and 0.61 mL/g ethylene gas, respectively, while 2% SFAC bubble gel only encapsulated 0.43 mL/g ethylene gas. This could be ascribed to two reasons. On the one hand, bubbles might collapse during gel network formation, leading to the gas escaping from the bubble carrier. On the other hand, the gas permeated the environment through the bubble shell and water layer. Thus, bubble stability was an important factor affecting the gas content of bubble gel. Compared to bubbles prepared with 2% SFAC, 3% and 4% SFAC bubbles had higher viscosity (Fig. 2), which could enhance the stability of the bubble cavity. Besides, 2% SFAC bubbles had the slowest gel formation speed because of the lowest molecule density and viscosity (Fig. 2b), resulting the disappearance and breakage of more bubble cavities during gel network formation. Thus, the gas concentration in 2% SFAC bubble gel was lower than that in 3% and 4% SFAC systems. However, the 6% SFAC bubble had the highest viscosity; the bubble cavity might be extruded by the gel network, resulting in bubble breakage, thus leading to gas escaping and the lowest ethylene gas content (0.22 mL/g) in bubble gel carriers.

The ethylene gas released from the bubble system during 60 h of storage is shown in Fig. 5b. The differing gas release rate in bubbles could be due to the gas permeability (Nguyen et al., 2020), shell materials, and bubble stability (Zahiri et al., 2021). Indeed, the bubble cavity stability showed a crucial impact on the gas release characteristics. The instabilized bubble cavity of the 2% bubble system showed a faster releasing rate. Although the 6% bubble system showed the highest viscosity, its bubbles could break faster due to extruding with a higher density of SFAC molecules, thus having a higher gas release rate. It can be seen that bubble carriers obtained with 4% SFAC (Fig. 5b) showed the lowest gas release speed, indicating that bubbles were relatively stable in this system. In order to further analyze the gas release kinetics from bubbles, the release process was fitted by Avrami's equation, and k and n parameters are shown in Table 2. The release rate constant k represented the speed of gas released from bubbles, dependent on bubble properties. The 4% SFAC bubble showed the smallest release rate constant k value (41.55), indicating the lowest release rate. While the highest release rate constant k value (727.49) was obtained from a 2% SFAC bubble system, in agreement with the release curve results (Fig. 5b). The n value is an important index of gas release mode. From Table 2, the n values of all bubble carriers fell between 0.34 and 0.86, showing a diffusion-limited process (Liu et al., 2023). That means gas released from bubbles mainly belongs to a major physical process (Shi et al., 2017b).

Table 2 Release rate constant (k), release parameter (n), and degree of fitting (R^2) for ethylene from bubble and bubble gel system based on Avrami's equation at room temperature.

Starch Concentration	Bubble system			Gel system		
	$k\times 10^{-3}$ (h^{-1})	n	R^2	$k\times 10^{-3}$ (h^{-1})	n	R^2
2%	727.49	0.34	0.991	357.08	0.44	0.999
3%	167.01	0.59	0.972	106.99	0.63	0.998
4%	41.55	0.86	0.995	17.53	0.99	0.998
6%	276.11	0.57	0.961	128.44	0.62	0.997

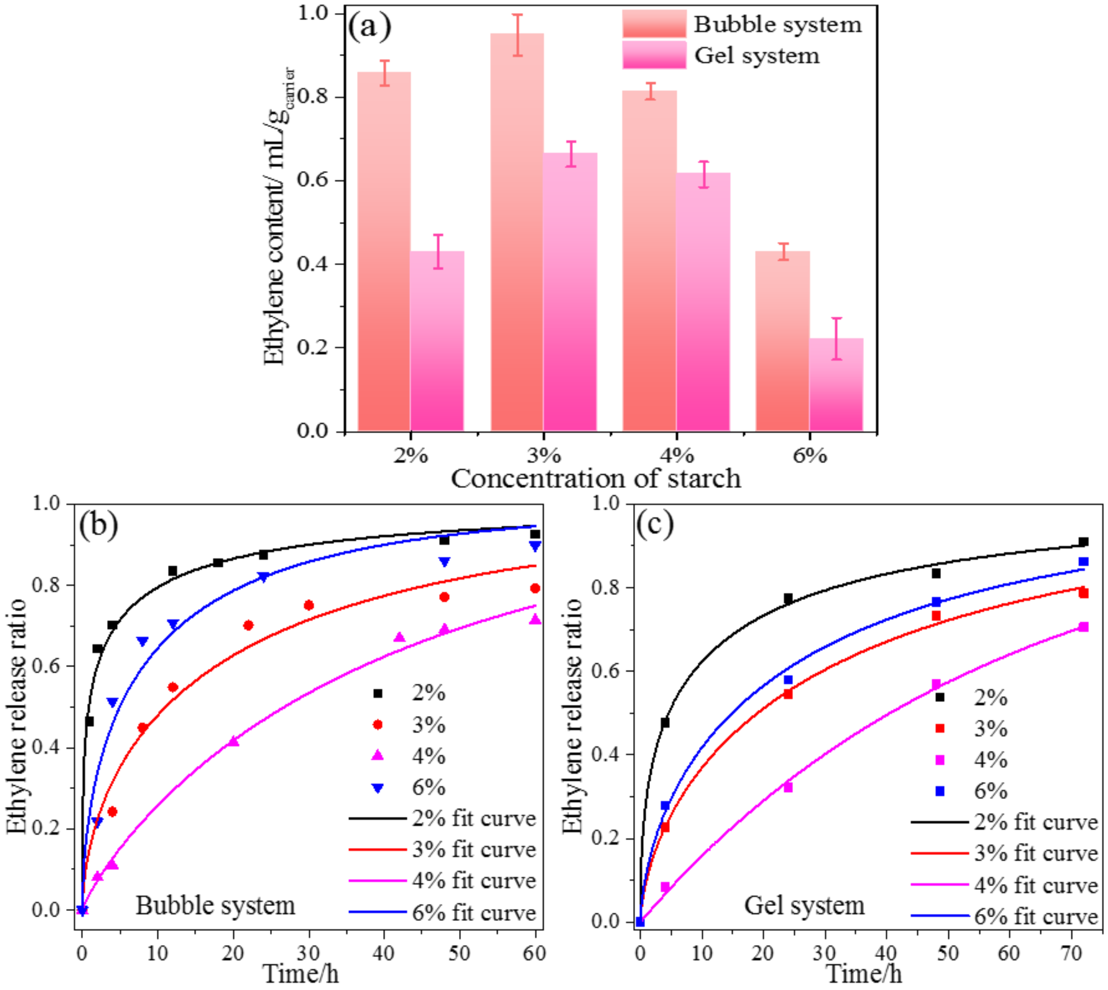

Fig. 5 The ethylene gas content (a) in fresh bubble and gel system, and gas release from bubble system (b) and bubble gel system (c) at room temperature.

In order to improve the stability of the bubble cavity and reduce the gas release rate, the bubble gel was designed and prepared. Fig. 5c shows the gas released from bubble gel. Similar to bubble carriers, the 4% SFAC bubble gel showed the lowest gas release speed, and the highest release rate was obtained in the 2% SFAC bubble gel. This could be due to the thicker bubble shell in the 4% SFAC gel system, which could retard gas release speed with the aid of the water layer. However, in the higher SFAC gel carriers (6%), the bubble might gradually break and disappear after gel formation because of extrusion, leading to faster gas escaping. Compared to release speed of bubbles (Fig. 5b), the gas release rate of bubble gel significantly decreased (Fig. 5c), indicating that bubble gel was a potential carrier for ethylene gas. The slow gas release speed could be attributed to two reasons. The first is that gel formation could immobilize bubble structure and improve bubble cavity stability. The other is that the bubble shell structure could be cross-linked by H^+ to form a physical barrier, preventing ethylene from escaping with the help of the water layer surrounding the bubble cavity. Meanwhile, Table 2 presented the parameters k and n. The parameter k values of bubble gel were obviously lower than those of their counterpart bubbles, further suggesting a lower release rate in bubble gel systems. According to the n values (0.44–0.99) of bubble gel, the gas release still belongs to the diffusion-limited mode, demonstrating the physical diffusion process through the bubble shell structure and water layer.

3.6. Gas loading mechanism of bubble gel

The schematic diagram of gas encapsulation in bubble and bubble gel systems is shown in Fig. 6. The bubble cavity formed with the help of Tween 80, which could load ethylene gas (Fig. 1 and Fig. 5). According to the gas release process from the bubble cavity, bubble stability was an important factor in slowing gas escaping. In order to improve the storage stability of bubbles, the bubble structure was immobilized to form bubble gel carrier. The SFAC molecules could interact with H^+ through cross-linking to form a gel network (Jiang et al., 2023). Thus, in this research, the bubble gel was gradually formed after SFAC molecules contacting with H^+, in which the H^+ was slowly released from D-(+)-gluconic acid δ-lactone in the bubble system. After bubble gel formation, the bubble cavities could decrease the gas leakage. On the one hand, the immobilized shell materials could wrap bubbles to prevent movement and breakage, increasing the stability of the gas carrier. On the other hand, the water films surrounding the bubble cavities to further retard ethylene gas from escaping.

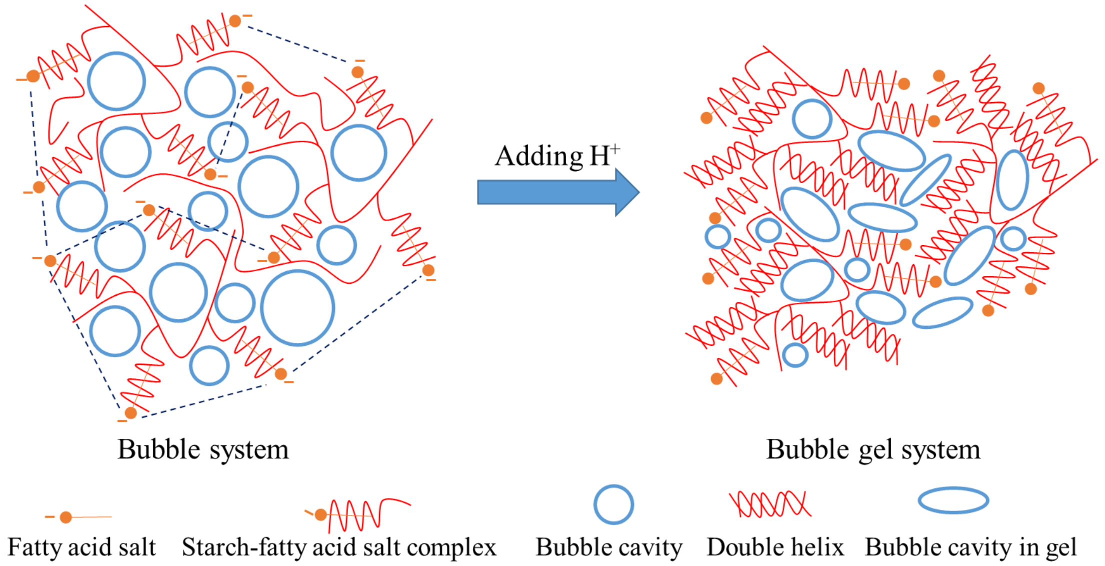

Fig. 6 Mechanism of ethylene gas encapsulation based on starch bubble.

4. Conclusion

In this research, we investigated the potential bubble and bubble gel gas carrier based on starch material. The all-bubble system had better encapsulation capacity with ethylene content from 0.43 to 0.95 mL/g. Bubble carriers prepared with different SFAC concentrations differed in the gas release speed. The 4% SFAC bubble showed suitable viscosity with the slowest gas release rate. Although 6% SFAC bubble showed the highest viscosity, but its gas release was faster than that of 3% and 4% SFAC, which might be due to bubble breakage by extrude in higher density of SFAC molecules, resulting gas escaping. In order to enhance the bubble cavity stability, the bubble gel carriers were prepared by adding D-(+)-gluconic acid δ-lactone, in which electrostatic repulsion between SFAC molecules disappeared, leading to form a gel network. Although the gas loading ability significantly decreased to 0.22–0.66 mL/g after bubble gel formation, the remaining ethylene was still capable of ripening effectively. Moreover, gas release speed of bubble gel carriers significantly decreased compared to counterpart bubble. These results could be ascribed to two reasons. The one is that bubble cavity was immobilized in gel to improve bubble stability. The other one is that water layer surrounded by bubble could also be a physical barrier to slow gas escaping. The bubble or bubble gel carrier is a potential material for gas encapsulation in the agriculture and food industry applications such as fruit ripening and food shelf-life regulation.

Conflict of Interest

The authors confirm that they have no conflicts of interest with respect to the work described in this manuscript

Acknowledgments

The authors acknowledge the financial support received from the National Natural Science Foundation of China (31771929), Guangdong Basic and Applied Basic Research Foundation (2023A1515012195), the 111 Project (B17018), the Chinese Scholarship Council (CSC) for funding as a joint PhD (202206150087) at Ghent University.

References

Agarwal, A., Ng, W.J., Liu, Y. (2011). Principle and applications of microbubble and nanobubble technology for water treatment. *Chemosphere,* 84, 1175-1180.

Arogundade, L.A., Mu, T.-H., Zhang, M., Chen, J.-W., Sun, H.-N., Zhang, D. (2021). Improving sweet potato protein gel properties through ε-(γ-glutamy)-lysine isopeptide cross-link catalyzed by transglutaminase. *Food Bioscience,* 39, 100828.

Azevedo, A., Etchepare, R., Calgaroto, S., Rubio, J. (2016). Aqueous dispersions of nanobubbles: Generation, properties and features. *Minerals Engineering,* 94, 29-37.

Binh, T., Joyce, Daryl, C., Yuwono, Talisa, D., Bhandari, Bhesh (2015). Controlled release of ethylene gas from the ethylene-alpha-cyclodextrin inclusion complex powder with deliquescent salts. *Journal of Inclusion Phenomena & Macrocyclic Chemistry,* 83, 281-288.

Chan, S.Y., Choo, W.S., Young, D.J., Loh, X.J. (2017). Pectin as a rheology modifier: Origin, structure, commercial production and rheology. *Carbohydrate Polymers,* 161, 118-139.

Chen, J., Cai, H., Zhang, M., Chen, Z. (2023). Effects of rice protein on the formation and structural properties of starch-lipid complexes in instant rice noodles incorporated with different fatty acids. *Food Bioscience,* 54, 102851.

Chen, L., Dai, Y., Hou, H., Wang, W., Ding, X., Zhang, H., Li, X., Dong, H. (2021). Effect of high pressure microfluidization on the morphology, structure and rheology of sweet potato starch. *Food Hydrocolloids,* 115, 106606.

Dodero, A., Vicini, S., Alloisio, M., Castellano, M. (2020). Rheological properties of sodium alginate solutions in the presence of added salt: an application of Kulicke equation. *Rheologica Acta,* 59, 365-374.

Dudu, O.E., Ma, Y., Olurin, T.O., Oyedeji, A.B., Oyeyinka, S.A., Ogungbemi, J.W. (2021). Changes in structural and functional characteristics of cassava flour by additive complexations stimulated by hydrothermal conditions. *Food Bioscience,* 43, 101289.

Fan, Z., Cheng, P., Gao, Y., Wang, D., Jia, G., Zhang, P., Prakash, S., Wang, Z., Han, J. (2022). Understanding the rheological properties of a novel composite salecan/gellan hydrogels. *Food Hydrocolloids,* 123, 107162.

Ferreira, L.S., Brito-Oliveira, T.C., Pinho, S.C. (2022). Emulsion-filled gels of soy protein isolate for vehiculation of vitamin D3: Effect of protein solubility on their mechanical and rheological characteristics. *Food Bioscience,* 45, 101455.

Friedman, A.J., Han, G., Navati, M.S., Chacko, M., Gunther, L., Alfieri, A., Friedman, J.M. (2008). Sustained release nitric oxide releasing nanoparticles: Characterization of a novel delivery platform based on nitrite containing hydrogel/glass composites. *Nitric Oxide,* 19, 12-20.

Ho, B.T., Joyce, D.C., Bhandari, B.R. (2011). Encapsulation of ethylene gas into α-cyclodextrin and characterisation of the inclusion complexes. *Food Chemistry,* 127, 572-580.

Hu, L., Xia, Z. (2018). Application of ozone micro-nano-bubbles to groundwater remediation. *Journal of Hazardous Materials,* 342, 446-453.

Huang, L., Li, S., Tan, C.P., Feng, Y., Zhang, B., Fu, X., Huang, Q. (2021). Solid encapsulation of lauric acid into “empty” V-type starch: Structural characteristics and emulsifying properties. *Carbohydrate Polymers,* 267, 118181.

Huang, X., Zheng, L., Xie, R. (2020). Effect of pre-harvest application of ethephon on colouration and expression of ripening related genes in citrus fruit. *The Journal of Horticultural Science and Biotechnology,* 96, 514-526.

Islam, M.N., Azemi, B.M.N.M. (1997). Rheological properties of calcium treated hydroxypropyl rice starches. *Starch – Stärke,* 49, 136-141.

Jay N. M., Janitha H. B., Shaini A.-H. (2017). Briefing: In situ decontamination of sediments using ozone nanobubbles and ultrasound. *Journal of Environmental Engineering and Science,* 12, 1-3.

Jeong, H., Park, J.-H., Shin, J.H., Yoo, J.-C., Park, C.Y., Hong, J. (2018). Prolonged release period of nitric oxide gas for treatment of bacterial keratitis by amine-rich polymer decoration of nanoparticles. *Chemistry of Materials,* 30, 8528-8537.

Jiang, Y., Junejo, S.A., Jia, X., Zhang, B., Fu, X., Huang, Q. (2023). Amylose content and pre-freezing regulate the structure and oil absorption of polyelectrolytes-based starch cryogel. *Carbohydrate Polymers,* 302, 120386.

Koev, T.T., Muñoz-García, J.C., Iuga, D., Khimyak, Y.Z., Warren, F.J. (2020). Structural heterogeneities in starch hydrogels. *Carbohydrate Polymers,* 249, 116834.

Li, H., Shi, L., Li, C., Fu, X., Huang, Q., Zhang, B. (2020). Metal-organic framework based on α-cyclodextrin gives high ethylene gas adsorption capacity and storage stability. *ACS Applied Materials & Interfaces,* 12, 34095-34104.

Lindner, J.R., Song, J., Christiansen, J., Klibanov, A.L., Xu, F., Ley, K. (2001). Ultrasound assessment of inflammation and renal tissue injury with microbubbles targeted to P-selectin. *Circulation,* 104, 2107-2112.

Liu, Z., Guo, X., Meng, H. (2020). Added ferulic acid enhances the emulsifying properties of pectins from different sources. *Food Hydrocolloids,* 100, 105439.

Liu, Z., Junejo, S.A., Zhang, B., Fu, X., Huang, Q. (2022a). Characteristics and ethylene encapsulation properties of V-type linear dextrin with different degrees of polymerisation. *Carbohydrate Polymers,* 277, 118814.

Liu, Z., Pi, F., Guo, X., Guo, X., Yu, S. (2019). Characterization of the structural and emulsifying properties of sugar beet pectins obtained by sequential extraction. *Food Hydrocolloids,* 88, 31-42.

Liu, Z., Shao, M., Junejo, S.A., Zhang, B., Jiang, H., Fu, X., Huang, Q. (2023). Controlled ethylene-releasing from V-type starch coated with sodium alginate for banana ripening via changing the humidity of environment. *Postharvest Biology and Technology,* 202, 112377.

Liu, Z., Wang, S., Tan, C.P., Zhang, B., Fu, X., Huang, Q. (2022b). Effect of lipids complexes on controlling ethylene gas release from V-type starch. *Carbohydrate Polymers,* 291, 119556.

McEwan, C., Owen, J., Stride, E., Fowley, C., Nesbitt, H., Cochrane, D., Coussios, C.C., Borden, M., Nomikou, N., McHale, A.P., Callan, J.F. (2015). Oxygen carrying microbubbles for enhanced sonodynamic therapy of hypoxic tumours. *Journal of Controlled Release,* 203, 51-56.

Montes, L., Santamaria, M., Garzon, R., Rosell, C.M., Moreira, R. (2022). Effect of the addition of different sodium alginates on viscoelastic, structural features and hydrolysis kinetics of corn starch gels. *Food Bioscience,* 47, 101628.

Muhammad, K., Mohd. Zahari, N.I., Gannasin, S.P., Mohd. Adzahan, N., Bakar, J. (2014). High methoxyl pectin from dragon fruit (Hylocereus polyrhizus) peel. *Food Hydrocolloids,* 42, 289-297.

Nair, R., Roy Choudhury, A. (2020). Synthesis and rheological characterization of a novel shear thinning levan gellan hydrogel. *International Journal of Biological Macromolecules,* 159, 922-930.

Nascimento, G.E.d., Simas-Tosin, F.F., Iacomini, M., Gorin, P.A.J., Cordeiro, L.M.C. (2016). Rheological behavior of high methoxyl pectin from the pulp of tamarillo fruit (Solanum betaceum). *Carbohydrate Polymers,* 139, 125-130.

Nguyen, T., Peng, Y., Seekell, R.P., Kheir, J.N., Polizzotti, B.D. (2020). Hyperbaric polymer microcapsules for tunable oxygen delivery. *Journal of Controlled Release,* 327, 420-428.

Peng, T., Britton, G.L., Kim, H., Cattano, D., Aronowski, J., Grotta, J., McPherson, D.D., Huang, S.-L. (2013). Therapeutic time window and dose dependence of xenon delivered via echogenic liposomes for neuroprotection in stroke. *CNS Neuroscience & Therapeutics,* 19, 773-784.

Schmidt, U.S., Koch, L., Rentschler, C., Kurz, T., Endreß, H.U., Schuchmann, H.P. (2015). Effect of molecular weight reduction, acetylation and esterification on the emulsification properties of citrus pectin. *Food Biophysics,* 10, 217-227.

Shen, J., Zhuo, N., Xu, S., Song, Z., Hu, Z., Hao, J., Guo, X. (2018). Resveratrol delivery by ultrasound-mediated nanobubbles targeting nucleus pulposus cells. *Nanomedicine,* 13, 1433-1446.

Shi, L., Fu, X., Huang, Q., Zhang, B. (2017a). Single helix in V-type starch carrier determines the encapsulation capacity of ethylene. *Carbohydrate Polymers,* 174, 798-803.

Shi, L., Fu, X., Tan, C.P., Huang, Q., Zhang, B. (2017b). Encapsulation of ethylene gas into granular cold-water-soluble starch: structure and release kinetics. *Journal of*

Agricultural and Food Chemistry, 65, 2189-2197.

Shi, L., Hopfer, H., Ziegler, G.R., Kong, L. (2019a). Starch-menthol inclusion complex: Structure and release kinetics. *Food Hydrocolloids,* 97, 105183.

Shi, L., Zhang, B., Li, C., Fu, X., Huang, Q. (2019b). Annealing improves the concentration and controlled release of encapsulated ethylene in V-type starch. *International Journal of Biological Macromolecules,* 141, 947-954.

Temesgen, T., Bui, T.T., Han, M., Kim, T.-i., Park, H. (2017). Micro and nanobubble technologies as a new horizon for water-treatment techniques: A review. *Advances in Colloid and Interface Science,* 246, 40-51.

Wu, Z., Chen, H., Dong, Y., Mao, H., Sun, J., Chen, S., Craig, V.S.J., Hu, J. (2008). Cleaning using nanobubbles: Defouling by electrochemical generation of bubbles. *Journal of Colloid and Interface Science,* 328, 10-14.

Yanes, M., Durán, L., Costell, E. (2002). Effect of hydrocolloid type and concentration on flow behaviour and sensory properties of milk beverages model systems. *Food Hydrocolloids,* 16, 605-611.

Zahiri, M., Taghavi, S., Abnous, K., Taghdisi, S.M., Ramezani, M., Alibolandi, M. (2021). Theranostic nanobubbles towards smart nanomedicines. *Journal of Controlled Release,* 339, 164-194.

Zhang, B., Luo, Y., Kanyuck, K., Bauchan, G., Mowery, J., Zavalij, P. (2016). Development of Metal–Organic Framework for Gaseous Plant Hormone Encapsulation To Manage Ripening of Climacteric Produce. *Journal of Agricultural and Food Chemistry,* 64, 5164-5170.

Zhu, J., An, H., Alheshibri, M., Liu, L., Terpstra, P.M.J., Liu, G., Craig, V.S.J. (2016). Cleaning with Bulk Nanobubbles. *Langmuir,* 32, 11203-11211.

Figure legend

Fig. 1 The size distribution and micrographs of fresh bubble system prepared by 2% (a), 3% (b), 4% (c), and 6% (d) starch dispersion.

Fig. 2 The changes in the viscosity (a) and shear stress (b) of dispersion and bubble system with the shear rate

Fig. 3 The strain sweep curves of gel (a) and bubble gel (b) system and the oscillatory frequency sweep curves of gel (c) and bubble gel (d) system.

Fig. 4 SEM images of gel system prepared with 3% (a), 4% (c), and 6% (e) starch dispersion, and bubble gel system prepared with 3% (b), 4% (d), and 6% (f) starch bubble system.

Fig. 5 The ethylene gas content (a) in fresh bubble and gel system, and gas release from bubble system (b) and bubble gel system (c) at room temperature.

Fig. 6 Mechanism of ethylene gas encapsulation based on starch bubble.